6th European Conference on Computational Mechanics (ECCM 6)
7th European Conference on Computational Fluid Dynamics (ECFD 7)
1115 June 2018, Glasgow, UK

COUPLING OF CONTINUOUS AND HDG METHODS

MAHENDRA PAIPURI[1,2], CARLOS TIAGO[1] AND SONIA FERNÁNDEZ–MÉNDEZ[2]

[1] CERIS, ICIST,
Instituto Superior Técnico,
Universidade de Lisboa, Av. Rovisco Pais,
1049-001 Lisboa, Portugal
{mahendra.paipuri, carlos.tiago}@tecnico.ulisboa.pt

[2] Laboratori de Càlcul Numèric (LaCàN),
Universitat Politècnica de Catalunya (UPC-BarcelonaTech),
08034 Barcelona, Spain
sonia.fernandez@upc.edu

Key words: hybridizable discontinuous Galerkin, continuous Galerkin, coupling, second-order elliptic, convergence

Abstract. A coupling strategy between hybridizable discontinuous Galerkin (HDG) and continuous Galerkin (CG) methods is proposed in the framework of second-order elliptic operators. The coupled formulation is implemented and its convergence properties are established numerically by using manufactured solutions. The influence of parameter, τ, on the coupled formulation is studied.

1 INTRODUCTION

Continuous Galerkin (CG) finite element methods are widely used in computational mechanics. However, for convection dominated problems, CG methods might pose stability issues. Discontinuous Galerkin (DG) finite element methods, originally developed for hyperbolic equations [9], offer some interesting features in this context: (i) local conservation, as they are based on satisfying conservation principles element-by-element, (ii) ability to handle hanging nodes, thereby making the implementation of adaptive algorithms relatively easier and (iii) ready parallelization. In addition, DG methods can be more robust than CG in convection dominated regimes. However, DG methods for problems involving self-adjoint operators are often criticised for having a higher number of degrees of freedoms (DOFs).

With the introduction of Hybridizable Discontinuous Galerkin (HDG) methods [3] in the framework of second-order elliptic problems, the mentioned drawback of the DG methods is addressed. The hybridization technique in the case of HDG methods leads to significant reduction in number of DOFs in the final system. HDG method have also been successfully applied to different governing equations with a very competitive number of DOFs when compared to CG methods [8].

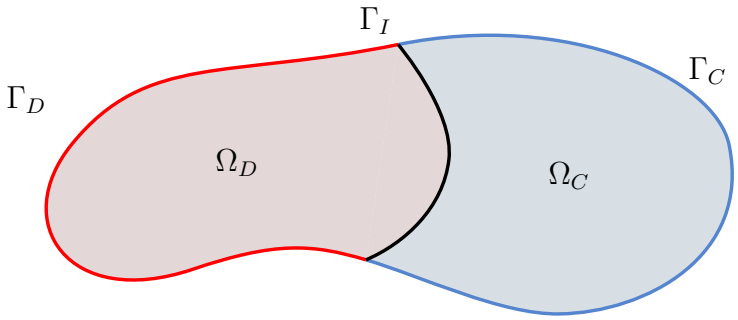

Figure 1: Domain representation: HDG and CG discretizations are considered in Ω_D and Ω_C, respectively.

As far as the knowledge of the authors, coupled CG-HDG scheme has not been proposed yet in any framework. Hence, the present work focuses on the coupling of HDG with CG in the context of heat equation, aiming to combine the favourable features of both CG and HDG methods. The present formulation is first step towards coupling HDG and CG discretization methods. The proposed coupled formulation can be extended for other governing equations like conjugate heat transfer problems [7].

2 NOTATION

Let the domain, Ω, be split into two sub-domains, Ω_D and Ω_C, such that $\bar{\Omega} = \bar{\Omega}_D \cup \bar{\Omega}_C$ with an interface $\Gamma_I = \bar{\Omega}_D \cap \bar{\Omega}_C$, as shown in fig. 1. In this work, HDG discretization will be considered in Ω_D, and CG formulation is stated in Ω_C. The domain Ω is assumed to be divided into n_{el} elements, Ω^e, with the boundaries $\partial\Omega^e$.

$$\bar{\Omega} = \bigcup_{e=1}^{n_{el}} \bar{\Omega}^e, \quad \Omega^e \cap \Omega^k = \emptyset \quad \text{for} \quad e \neq k, \tag{1}$$

The elements in Ω_D and Ω_C are represented as Ω_D^e and Ω_C^e, respectively, while the exterior boundaries are denoted by Γ_D and Γ_C, respectively. The union of all faces in Ω_D is denoted as

$$\Gamma = \bigcup_{e=1}^{m_{el}} \partial\Omega_D^e, \tag{2}$$

where m_{el} is the number of elements in Ω_D.

3 CG-HDG COUPLED FORMULATION FOR THE HEAT EQUATION

This section presents suitable formulations for the solution of the heat equation coupling HDG discretization in Ω_D and CG discretization in Ω_C.

3.1 Governing equations

The heat equation in Ω_D and Ω_C, along with the transmission conditions on Γ_I, are

$$\begin{aligned}
\boldsymbol{q}_D + (k_D \operatorname{grad} \theta_D) &= \mathbf{0} && \text{in} \quad \Omega_D, && \text{(3a)}\\
\operatorname{div} \boldsymbol{q}_D &= \bar{g}_D && \text{in} \quad \Omega_D, && \text{(3b)}\\
-\operatorname{div}\ (k_C \operatorname{grad} \theta_C) &= \bar{g}_C && \text{in} \quad \Omega_C, && \text{(3c)}\\
\theta_D &= \bar{\theta}_D && \text{on} \quad \Gamma_D, && \text{(3d)}\\
\theta_C &= \bar{\theta}_C && \text{on} \quad \Gamma_C, && \text{(3e)}\\
\theta_D - \theta_C &= 0 && \text{on} \quad \Gamma_I, && \text{(3f)}\\
\boldsymbol{q}_D \cdot \boldsymbol{n}_D - (k_C \operatorname{grad} \theta_C) \cdot \boldsymbol{n}_C &= 0 && \text{on} \quad \Gamma_I, && \text{(3g)}
\end{aligned}$$

where θ_D and θ_C are the temperatures in Ω_D and Ω_C, respectively and $\boldsymbol{q}_D$ is the independently approximated flux in Ω_D. Heat conductivity coefficients are denoted by k_D, k_C, heat generations per unit volume are given by $\bar{g}_D$, $\bar{g}_C$, where the subscripts D and C denote that quantities are defined in Ω_D and Ω_C, respectively. Unit normal vectors on Γ_I, $\boldsymbol{n}_D$ and $\boldsymbol{n}_C$, are outward vectors to Ω_D and Ω_C, respectively, which satisfy $\boldsymbol{n}_D = -\boldsymbol{n}_C$. Dirichlet boundary conditions are prescribed with values $\bar{\theta}_D$ and $\bar{\theta}_C$ for both sub-domains on the exterior boundaries to simplify the presentation. The extension of the formulation to problems including Neumann boundary conditions on the exterior boundary is straightforward following the usual procedure for HDG or CG formulations.

Equation (3f) represents the continuity of θ, whereas (3g) states the equilibrium of the normal flux across the interface.

3.2 Weak formulation of the CG-HDG coupled problem

As shown in fig. 2, in Ω_C the temperature field, θ_C, is approximated with a continuous space on the mesh represented in blue, while in the HDG domain, Ω_D, the elemental variables θ_D and $\boldsymbol{q}_D$ are approximated within each element represented in green and a new independently approximated trace variable, $\hat{\theta}_D$, is defined along the red edges (mesh skeleton).

The CG weak form of the heat equation in Ω_C is,

$$(\operatorname{grad} \delta\theta_C, k_C \operatorname{grad} \theta_C)_{\Omega_C} - \langle \delta\theta_C, k_C (\operatorname{grad} \theta_C \cdot \boldsymbol{n}_C) \rangle_{\Gamma_I} - (\delta\theta_C, \bar{g}_C)_{\Omega_C} = 0, \tag{4}$$

where $\delta\theta_C = 0$ on Γ_C. Equation (4) is obtained after multiplying equation (3c) with $\delta\theta_C$ and performing integration by parts.

For the HDG domain, Ω_D, the discrete problem is expressed as element-by-element local problems and the so-called global problem (see [3] for more details). Note that the only difference of equations (7) with the standard HDG local problem is that the Dirichlet data, that is imposed in weak is

$$\theta_D = \begin{cases} \hat{\theta}_D & \text{on } \partial\Omega_D^e \backslash \Gamma_I, \\ \theta_C & \text{on } \partial\Omega_D^e \cap \Gamma_I. \end{cases} \tag{5}$$

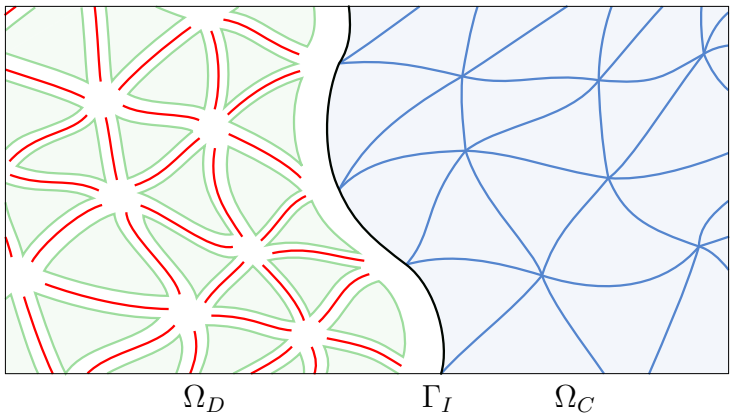

Figure 2: Representation of a computational mesh for coupled discretization. *Green* triangles represent the HDG local elemental variables while the *red* edges correspond to HDG trace variable. CG mesh is represented in *blue* and Γ_I is represented in *black*.

For the elements along the interface, no trace variables are considered, as illustrated in fig. 2. For elements in the interior of Ω_D, the local problem is the standard one, with a weak imposition of $\theta_D = \hat{\theta}_D$ on $\partial\Omega_D^e$. The Dirichlet boundary condition (5) ensures the weak continuity of the temperature, *i.e.*, the transmission condition (3f) on Γ_I. The HDG numerical normal flux, $\hat{\boldsymbol{q}}_D \cdot \boldsymbol{n}$, is defined as,

$$\hat{\boldsymbol{q}}_D \cdot \boldsymbol{n} = \begin{cases} \boldsymbol{q}_D \cdot \boldsymbol{n} + \tau(\theta_D - \hat{\theta}_D) & \text{on } \partial\Omega_D^e \backslash \Gamma_I, \\ \boldsymbol{q}_D \cdot \boldsymbol{n}_D + \tau(\theta_D - \theta_C) & \text{on } \partial\Omega_D^e \cap \Gamma_I. \end{cases} \tag{6}$$

Therefore, the *local problem* in each element can be written as,

$$\begin{aligned} (\delta\theta_D, \operatorname{div} \boldsymbol{q}_D)_{\Omega_D^e} + \left\langle \delta\theta_D, \tau(\theta_D - \hat{\theta}_D) \right\rangle_{\partial\Omega_D^e \backslash \Gamma_I} \\ + \langle \delta\theta_D, \tau(\theta_D - \theta_C) \rangle_{\partial\Omega_D^e \cap \Gamma_I} - (\delta\theta_D, \bar{g}_D)_{\Omega_D^e} = 0, \\ \left(\delta\boldsymbol{q}_D, k_D^{-1}\boldsymbol{q}_D\right)_{\Omega_D^e} - (\operatorname{div} \delta\boldsymbol{q}_D, \theta_D)_{\Omega_D^e} + \left\langle \delta\boldsymbol{q}_D \cdot \boldsymbol{n}, \hat{\theta}_D \right\rangle_{\partial\Omega_D^e \backslash \Gamma_I} \\ + \langle \delta\boldsymbol{q}_D \cdot \boldsymbol{n}_D, \theta_C \rangle_{\partial\Omega_D^e \cap \Gamma_I} = 0, \end{aligned} \tag{7}$$

where $\hat{\theta}_D$ is an independently approximated trace variable along the mesh skeleton, Γ, which is represented in red in fig. 2, and τ is a stabilization parameter of order $\mathcal{O}(k_D)$. Parameter τ has an important effect on stability, accuracy and convergence properties of the HDG method (see [2, 6]). As usual in HDG, the local problem can be solved element-by-element to express θ_D and $\boldsymbol{q}_D$ in terms of $\hat{\theta}_D$ and, in the present case, θ_C as well.

The *global problem* in Ω_D is the usual HDG global problem, which can be presented as

$$\sum_{e=1}^{m_{el}} \left\langle \delta\hat{\theta}_D, \hat{\boldsymbol{q}}_D \cdot \boldsymbol{n} \right\rangle_{\partial\Omega_D^e \setminus \Gamma_I} = 0, \tag{8a}$$

$$\hat{\theta}_D = \mathbb{P}_2(\bar{\theta}_D) \quad \text{on } \Gamma_D, \tag{8b}$$

where $\delta\hat{\theta}_D = 0$ on Γ_D, $\mathbb{P}_2(\bar{\theta}_D)$ is the $\mathcal{L}_2$ projection of the Dirichlet data into the approximation space on Γ_D.

Essentially, the global problem (8a) states the so-called conservativity condition, *i.e*, the weak continuity of the normal flux across all the interior faces of the mesh in Ω_D. The continuity of the fluxes on the interface, Γ_I, *i.e.*, equation (3g), is imposed between the numerical normal flux of HDG, $\hat{\boldsymbol{q}}_D \cdot \boldsymbol{n}_D$, which is defined in equation (6) and the flux on the interface from Ω_C, which is $-k_C \operatorname{grad} \theta_C \cdot \boldsymbol{n}_C$, leading to,

$$-\langle \delta\theta_C, \boldsymbol{q}_D \cdot \boldsymbol{n}_D + \tau(\theta_D - \theta_C) \rangle_{\Gamma_I} + \langle \delta\theta_C, k_C \operatorname{grad} \theta_C \cdot \boldsymbol{n}_C \rangle_{\Gamma_I} = 0. \tag{9}$$

By summing equation (9) to the weak form of CG in Ω_C (4), and using the weak formulation of HDG, (7) and (8), in Ω_D, the coupled discrete problem is obtained: find $(\boldsymbol{q}_D, \theta_D, \hat{\theta}_D, \theta_C) \in \left[\mathcal{V}^h\right]^d \times \mathcal{V}^h \times \Lambda^h \times \mathcal{V}_c^h$ such that $\hat{\theta}_D = \mathbb{P}_2(\bar{\theta}_D)$ on Γ_D, $\theta_C = \Pi^h(\bar{\theta}_C)$ on Γ_C and

$$\begin{aligned}
&(\delta\theta_D, \operatorname{div} \boldsymbol{q}_D)_{\Omega_D^e} + \left\langle \delta\theta_D, \tau(\theta_D - \hat{\theta}_D) \right\rangle_{\partial\Omega_D^e \setminus \Gamma_I} \\
&\qquad + \langle \delta\theta_D, \tau(\theta_D - \theta_C) \rangle_{\partial\Omega_D^e \cap \Gamma_I} - (\delta\theta_D, \bar{g}_D)_{\Omega_D^e} = 0, \\
&\left(\delta\boldsymbol{q}_D, k_D^{-1}\boldsymbol{q}_D\right)_{\Omega_D^e} - (\operatorname{div} \delta\boldsymbol{q}_D, \theta_D)_{\Omega_D^e} + \left\langle \delta\boldsymbol{q}_D \cdot \boldsymbol{n}, \hat{\theta}_D \right\rangle_{\partial\Omega_D^e \setminus \Gamma_I} \\
&\qquad + \langle \delta\boldsymbol{q}_D \cdot \boldsymbol{n}_D, \theta_C \rangle_{\partial\Omega_D^e \cap \Gamma_I} = 0,
\end{aligned} \tag{10a}$$

for $e = 1, \ldots, m_{el}$ and,

$$\sum_{e=1}^{m_{el}} \left\langle \delta\hat{\theta}_D, \left(\boldsymbol{q}_D \cdot \boldsymbol{n} + \tau(\theta_D - \hat{\theta}_D) \right) \right\rangle_{\partial\Omega_D^e \setminus \Gamma_I} = 0, \tag{10b}$$

$$\begin{aligned}
&(\operatorname{grad} \delta\theta_C, k_C \operatorname{grad} \theta_C)_{\Omega_C} - \langle \delta\theta_C, \boldsymbol{q}_D \cdot \boldsymbol{n}_D + \tau\left(\theta_D - \theta_C\right) \rangle_{\Gamma_I} \\
&\qquad - (\delta\theta_C, \bar{g}_C)_{\Omega_C} = 0.
\end{aligned} \tag{10c}$$

for all $(\delta\boldsymbol{q}_D, \delta\theta_D, \delta\hat{\theta}_D, \delta\theta_C) \in \left[\mathcal{V}^h\right]^d \times \mathcal{V}^h \times \Lambda^h \times \mathcal{V}_c^h$ such that $\delta\hat{\theta}_D = 0$ on Γ_D and $\delta\theta_C = 0$ on Γ_C, where the discrete spaces are defined as

$$\begin{aligned}
\mathcal{V}^h &:= \left\{ v \in \mathcal{L}_2(\Omega_D) \ : \ v|_{\Omega^e} \in \mathcal{P}_k(\Omega^e), \forall\, \Omega^e \subset \Omega_D \right\}, \\
\Lambda^h &:= \left\{ \hat{v} \in \mathcal{L}_2(\Gamma \setminus \Gamma_I) \ : \ \hat{v}|_{\Gamma_i} \in \mathcal{P}_k(\Gamma_i), \forall\, \Gamma_i \subset \Gamma \right\}, \\
\mathcal{V}_c^h &:= \left\{ v \in \mathcal{H}^1(\Omega_C) \ : \ v|_{\Omega^e} \in \mathcal{P}_r(\Omega^e), \forall\, \Omega^e \subset \Omega_C \right\}.
\end{aligned} \tag{11}$$

As usual in HDG, the spaces for approximation in Ω_D, $\mathcal{V}^h$ and Λ^h, consider polynomials of the same degree k for all variables. Numerical tests in section 3.4 show that the HDG

super-convergence cannot be retained by the coupling with the CG approximation of same degree, $r = k$. However, as expected, convergence rates of order $k + 2$ for the solution, and of order $k + 1$ for the flux, are obtained when higher degree $r = k + 1$ is considered for the CG approximation space $\mathcal{V}_c^h$.

The discretization of the system of equations in (10) gives rise to a matrix equation of the form

$$\left[\begin{array}{cc:cc} \mathbf{A}_{\hat{\theta}\hat{\theta}} & \mathbf{0} & \mathbf{A}_{\hat{\theta}\theta} & \mathbf{A}_{\hat{\theta}q} \\ \mathbf{0} & \mathbf{K}_{\theta\theta} & \mathbf{B}_{\theta\theta}^T & \mathbf{B}_{\theta q} \\ \hdashline \mathbf{A}_{\theta\hat{\theta}} & \mathbf{B}_{\theta\theta} & \mathbf{A}_{\theta\theta} & \mathbf{A}_{\theta q} \\ \mathbf{A}_{q\hat{\theta}} & \mathbf{B}_{q\theta} & \mathbf{A}_{q\theta} & \mathbf{A}_{qq} \end{array}\right] \left\{\begin{array}{c} \hat{\boldsymbol{\theta}}_D \\ \boldsymbol{\theta}_C \\ \hdashline \boldsymbol{\theta}_D \\ \mathbf{q}_D \end{array}\right\} = \left\{\begin{array}{c} \mathbf{0} \\ \bar{\mathbf{g}}_C \\ \hdashline \bar{\mathbf{g}}_D \\ \mathbf{0} \end{array}\right\}. \tag{12}$$

The column vectors $\boldsymbol{\theta}_D, \mathbf{q}_D, \hat{\boldsymbol{\theta}}_D$ and $\boldsymbol{\theta}_C$ contain the DOFs associated to $\theta_D, \boldsymbol{q}_D, \hat{\theta}_D$ and θ_C, respectively. Static condensation is assumed for the CG discretization, expressing the nodal values of interior nodes of the element in terms of the nodal values on the edges.

3.3 Alternative CG-HDG coupled formulation with a projection operator on the interface

The coupled formulation presented earlier considers the standard HDG local problem for the elements that do not share the interface, $\partial\Omega_D^e \cap \Gamma_I = \emptyset$, and a non-standard HDG local problem imposing (5) in weak form for elements along the interface, $\partial\Omega_D^e \cap \Gamma_I \neq \emptyset$. In terms of implementation, additional matrices, $\mathbf{B}_{\theta\theta}$ and $\mathbf{B}_{\theta q}$, in the elements along the interface boundary Γ_I are needed for the non-standard HDG local solver. An alternative coupling formulation is proposed in this section to keep the implementation changes to minimum in any existing HDG and CG codes. The main idea in this formulation is to use a projection to satisfy the transmission conditions. This formulation only requires the standard elemental matrices from HDG (after static condensation of local variables into trace variable) and CG domains, and a projection operation is used on the HDG elemental matrices before assembling into the global system. This requires minimal changes to the existing codes and it is noticed that, in the numerical results, this implementation gives practically the same results as the earlier one with same convergence rates.

In this case, the Dirichlet boundary conditions for the local problem are defined as follows,

$$\theta_D = \begin{cases} \hat{\theta}_D & \text{on } \partial\Omega_D^e \backslash \Gamma_I, \\ \mathbb{P}_2(\theta_C) & \text{on } \partial\Omega_D^e \cap \Gamma_I, \end{cases} \tag{13}$$

where in equation (13) the operator $\mathbb{P}_2$ stands for the $\mathcal{L}_2$ projection from the CG space $\mathcal{V}_c^h$ to the HDG space $\mathcal{V}^h$. Hence, the trace is set to the projection of the CG solution on the faces along the interface, *i.e.*, $\hat{\theta}_D = \mathbb{P}_2(\theta_C)$ on $\partial\Omega_D^e \cap \Gamma_I$. Consequently, the numerical normal flux is defined as,

$$\hat{\boldsymbol{q}}_D \cdot \boldsymbol{n} = \begin{cases} \boldsymbol{q}_D \cdot \boldsymbol{n} + \tau(\theta_D - \hat{\theta}_D) & \text{on } \partial\Omega_D^e \backslash \Gamma_I, \\ \boldsymbol{q}_D \cdot \boldsymbol{n}_D + \tau(\theta_D - \mathbb{P}_2(\theta_C)) & \text{on } \partial\Omega_D^e \cap \Gamma_I. \end{cases} \tag{14}$$

The jump of fluxes along the interface is weighted with $\mathbb{P}_2\left(\delta\theta_C\right)$ leading to,

$$-\left\langle \mathbb{P}_2\left(\delta\theta_C\right), \boldsymbol{q}_D \cdot \boldsymbol{n}_D + \tau\left(\theta_D - \mathbb{P}_2\left(\theta_C\right)\right)\right\rangle_{\Gamma_I} + \left\langle \mathbb{P}_2\left(\delta\theta_C\right), k_C \operatorname{grad}\theta_C \cdot \boldsymbol{n}_C\right\rangle_{\Gamma_I} = 0. \tag{15}$$

Using (13) and (15), the weak formulation of the coupled discrete problem becomes: find $(\boldsymbol{q}_D, \theta_D, \hat{\theta}_D, \theta_C) \in \left[\mathcal{V}^h\right]^d \times \mathcal{V}^h \times \Lambda^h \times \mathcal{V}_c^h$ such that $\hat{\theta}_D = \mathbb{P}_2(\bar{\theta}_D)$ on Γ_D, $\theta_C = \Pi^h(\bar{\theta}_C)$ on Γ_C and

$$\begin{aligned}
&(\delta\theta_D, \operatorname{div} \boldsymbol{q}_D)_{\Omega_D^e} + \left\langle \delta\theta_D, \tau(\theta_D - \hat{\theta}_D) \right\rangle_{\partial\Omega_D^e \setminus \Gamma_I} \\
&\qquad + \langle \delta\theta_D, \tau(\theta_D - \mathbb{P}_2(\theta_C)) \rangle_{\partial\Omega_D^e \cap \Gamma_I} - (\delta\theta_D, \bar{g}_D)_{\Omega_D^e} = 0, \\
&\left(\delta\boldsymbol{q}_D, k_D^{-1}\boldsymbol{q}_D\right)_{\Omega_D^e} - (\operatorname{div} \delta\boldsymbol{q}_D, \theta_D)_{\Omega_D^e} + \left\langle \delta\boldsymbol{q}_D \cdot \boldsymbol{n}, \hat{\theta}_D \right\rangle_{\partial\Omega_D^e \setminus \Gamma_I} \\
&\qquad + \langle \delta\boldsymbol{q}_D \cdot \boldsymbol{n}_D, \mathbb{P}_2(\theta_C) \rangle_{\partial\Omega_D^e \cap \Gamma_I} = 0,
\end{aligned} \tag{16a}$$

for $e = 1, \ldots, m_{el}$ and,

$$\sum_{e=1}^{m_{el}} \left\langle \delta\hat{\theta}_D, \left(\boldsymbol{q}_D \cdot \boldsymbol{n} + \tau(\theta_D - \hat{\theta}_D)\right) \right\rangle_{\partial\Omega_D^e \setminus \Gamma_I} = 0, \tag{16b}$$

$$\begin{aligned}
&(\operatorname{grad} \delta\theta_C, k_C \operatorname{grad} \theta_C)_{\Omega_C} - \langle \mathbb{P}_2(\delta\theta_C), \boldsymbol{q}_D \cdot \boldsymbol{n}_D + \tau(\theta_D - \mathbb{P}_2(\theta_C)) \rangle_{\Gamma_I} \\
&\qquad + \langle (\mathbb{P}_2(\delta\theta_C) - \delta\theta_C), k_C \operatorname{grad} \theta_C \cdot \boldsymbol{n}_C \rangle_{\Gamma_I} - (\delta\theta_C, \bar{g}_C)_{\Omega_C} = 0.
\end{aligned} \tag{16c}$$

for all $(\delta\boldsymbol{q}_D, \delta\theta_D, \delta\hat{\theta}_D, \delta\theta_C) \in \left[\mathcal{V}^h\right]^d \times \mathcal{V}^h \times \Lambda^h \times \mathcal{V}_c^h$ such that $\delta\hat{\theta}_D = 0$ on Γ_D and $\delta\theta_C = 0$ on Γ_C.

The weak form in equations (16) is similar to one presented earlier in equations (10) except for two major differences. First, θ_C is now replaced by its projection, $\mathbb{P}_2(\theta_C)$, in the HDG local problems (16a), and an additional term $\langle (\mathbb{P}_2(\delta\theta_C) - \delta\theta_C), k_C \operatorname{grad} \theta_C \cdot \boldsymbol{n}_C \rangle_{\Gamma_I}$ appears in the last equation (16c). The implementation of this new term maybe cumbersome, because it requires the computation of the gradient of the CG elemental basis functions on the integration points on the interface. However, $\mathbb{P}_2(\delta\theta_C) - \delta\theta_C = \mathcal{O}(h^{k+1})$, where h is the mesh size and k is degree of approximation, and therefore, this term can be safely neglected in the discrete problem without losing neither the convergence nor the accuracy of the solution.

This formulation does not require the computation of the new matrices that arise in (10), namely $\mathbf{B}_{\theta\theta}$ and $\mathbf{B}_{\theta q}$. The projection operation can be done in an element-by-element basis on the HDG elemental matrices for the elements along the interface boundary. For the sake of simplifying the presentation the nodal values of the CG approximation, $\boldsymbol{\theta}_C$, are split into values for nodes on the interface, $\boldsymbol{\theta}_C^I$, and the remaining CG nodal values, $\boldsymbol{\theta}_C^i$. The global stiffness matrix can be then represented as,

$$\begin{bmatrix} \mathbf{K}_{DD} & \mathbf{K}_{DI}\mathbf{P} & \mathbf{0} \\ \mathbf{P}^T\mathbf{K}_{ID} & \mathbf{P}^T\mathbf{K}_{II}^D\mathbf{P} + \mathbf{K}_{II}^C & \mathbf{K}_{IC} \\ \mathbf{0} & \mathbf{K}_{CI} & \mathbf{K}_{CC} \end{bmatrix} \begin{Bmatrix} \hat{\boldsymbol{\theta}}_D \\ \boldsymbol{\theta}_C^I \\ \boldsymbol{\theta}_C^i \end{Bmatrix} = \begin{Bmatrix} \mathbf{f}_D \\ \mathbf{P}^T\mathbf{f}_I^D + \mathbf{f}_I^C \\ \mathbf{f}_C \end{Bmatrix}, \tag{17}$$

where in equation (17), $\mathbf{P}$ is the assembly of projection matrices on all the faces along the interface. This implementation can be easily plugged into any existing HDG solver for heat equation.

Both coupled formulations (10) and (16) have been implemented and the comparison of the numerical results inferred that both are practically identical. In some tests, the first proposed formulation (10) gave slightly smaller errors. The difference might be due to neglecting the term $\mathbb{P}_2(\delta\theta_C) - \delta\theta_C$ in the last formulation (16). However, the difference in the errors — even for the coarsest mesh — is negligible and, hence, in all the results presented in this work, the formulation with projection (16) is used neglecting the term $\mathbb{P}_2(\delta\theta_C) - \delta\theta_C$.

3.4 Convergence

In this section, the convergence results of the coupled CG-HDG formulation for the heat equation are presented. A square domain, $\Omega := [0,1]^2$ is considered with the analytical solution,

$$\theta = 1 + \cos(\pi x_1)\cos(\pi x_2). \tag{18}$$

Dirichlet boundary conditions are prescribed on all the exterior boundary.

The domain is divided into two halves in vertical direction. The domain corresponding to HDG is $\Omega_D := [0, 0.5] \times [0, 1]$, the CG domain is $\Omega_C := [0.5, 1] \times [0, 1]$, and the interface, Γ_I, is $x_1 = 0.5$. A suitable body force is computed from the heat equation with the considered analytical solution for both domains, with the conductivity constants, $k_C = k_D = 1$.

Meshes are obtained by splitting a regular $n \times n$ Cartesian grid into $2n^2$ triangles, which gives an uniform mesh element size, $h = 1/n$. The results presented here consider a parameter of $\tau = 1$ on all faces of each element in HDG domain, Ω_D.

Figure 3 shows the convergence for the coupled formulation with same degree for CG and HDG, with $k = 1 - 8$ and element size, $h = 0.5/\{1, 2, 4, 8, 16\}$. The error in θ is measured by using $\mathcal{L}_2$ norm of errors of the post-processed solution, θ_D^*, in Ω_D, and CG solution, θ_C, in Ω_C. Similarly, error in $\operatorname{grad}\theta$ is computed using $\mathcal{L}_2$ norm of error in $\boldsymbol{q}_D$ in Ω_D and error in $\operatorname{grad}\theta_C$ in Ω_C.

When the degree of approximation k is used for both HDG and CG domains, even though HDG has superior convergence properties, errors in CG domain dominates for both θ and $\operatorname{grad}\theta$. Hence, as shown in fig. 3a, the order of convergence of the coupled solution is $k+1$ for θ. Similarly, for $\operatorname{grad}\theta$, the order of convergence is k.

Figure 4 shows the convergence of θ_D^* and $\boldsymbol{q}_D$ in Ω_D for the coupled CG(P_k)-HDG(P_k) model. Sub-optimal convergence rates are observed in both variables: for $k > 2$, θ_D^* converges with only $k + 1.5$ instead of $k + 2$, and $\boldsymbol{q}_D$ converges with order $k + 0.5$ instead of $k + 1$. HDG super-convergence requires a solution of order $k + 1$ for $\boldsymbol{q}_D$, and mean of θ_D that converges with order $k + 2$ in each element in Ω_D. The elements in Ω_D that share the interface, Γ_I, do not possess the mentioned convergence rates because of the coupling with CG domain, Ω_C.

To address this shortcoming, higher degree of approximation is considered for the CG discretization. Figure 5a shows the convergence plots for a coupled approximation with degree k for HDG and degree $k + 1$ for CG. Optimal convergence rates of both methods are retained in this case. The post-processed solution of HDG with degree k has the same

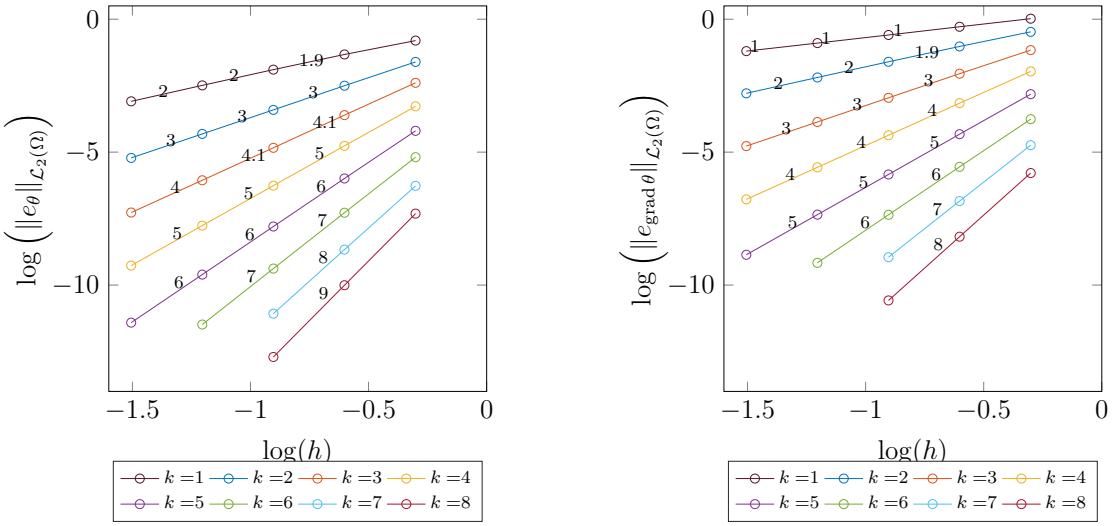

(a) θ. (b) $\operatorname{grad}\theta$.

Figure 3: Coupled CG(P_k)-HDG(P_k): convergence plots in Ω.

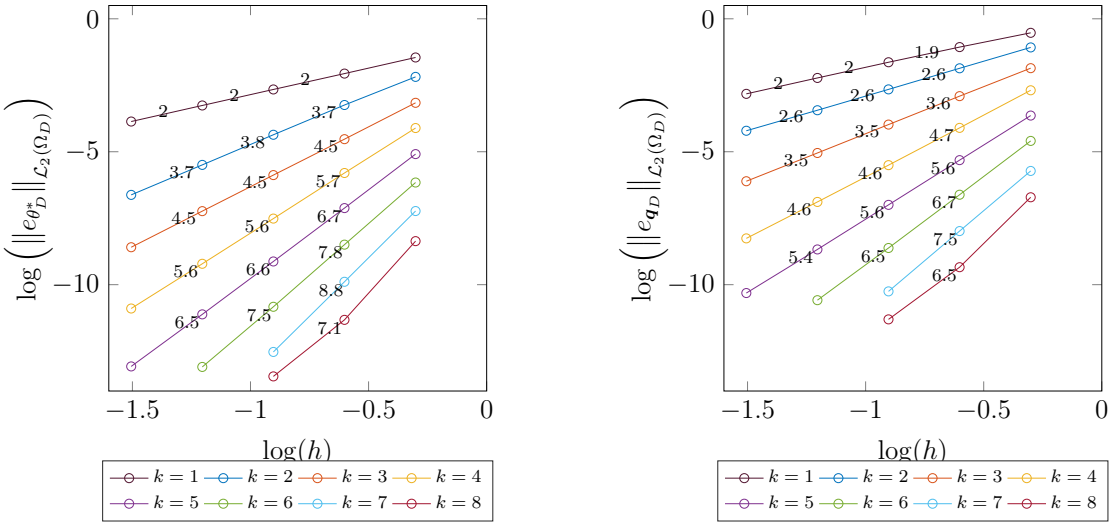

(a) θ_D^*. (b) $\boldsymbol{q}_D$.

Figure 4: Coupled CG(P_k)-HDG(P_k): convergence plots in Ω_D.

order of convergence, which is $k+2$, as the CG solution with degree $k+1$. Similarly, the flux $\boldsymbol{q}_D$ of HDG converges with same order as $\operatorname{grad}\theta_C$ of CG, which is $k+1$.

The same conclusions are drawn for quadrilateral elements as well and, hence, the results are omitted.

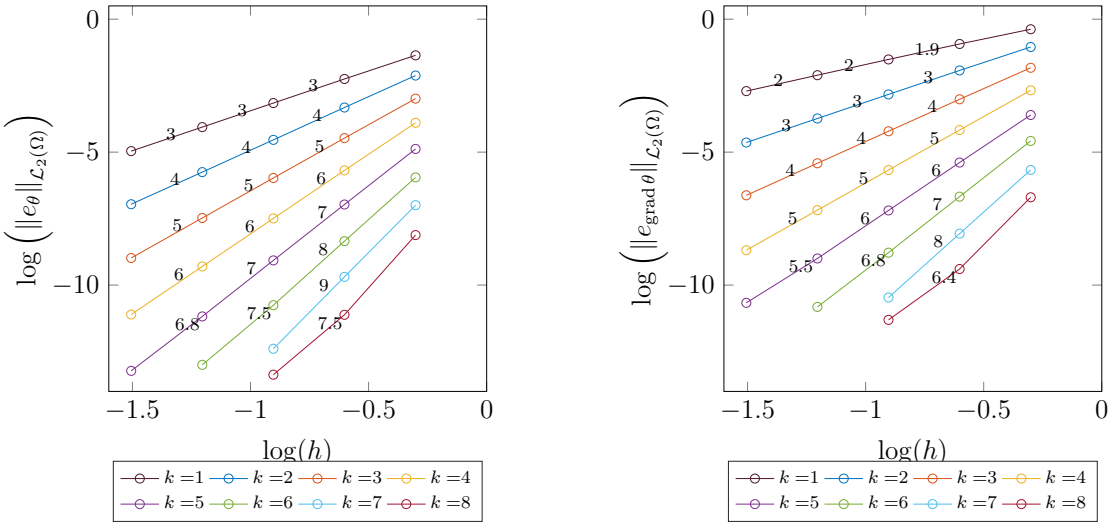

(a) θ. (b) grad θ.

Figure 5: Coupled CG(P_{k+1})-HDG(P_k): convergence plots in Ω.

3.5 Influence of τ parameter on coupled formulation

This section presents the study of effect of parameter, τ, on the coupled formulation. Two different cases are considered in this study namely, single-face [1] and all-face [4] techniques. In all-face approach, τ is a positive value for all the edges of each element whereas, in single-face approach, τ is zero on all edges except an arbitrarily chosen edge of each element. The convergence results presented earlier use all-face approach. However, previous works [2, 5] conclude that the method is less sensitive to the choice of τ with the single-face definition, resulting in a more robust formulation than all-face approach in the case of second-order elliptic operators. Hence, both cases are investigated in the context of the present coupled formulation.

Figures 6 and 7 show the convergence of temperature and gradient of temperature for different values of τ, for single-face and all-face approach, respectively. The results are in agreement with the conclusions in [5]. In the case of single-face approach, the error values are practically the same for different values of τ. It can also be noticed that optimal rates of convergence are achieved for both temperature and gradient of temperature. It is worthy to note that it is possible to take $\tau = 0$ on all faces sharing the interface without loss of neither convergence nor accuracy in the single-face approach. However, in the case of all-face approach, as the parameter, τ, is increased, the optimal rate of convergence is lost. From fig. 7, it is clear that both temperature and gradient of temperature show sub-optimal convergence for τ significantly larger than 1, due to loss of optimal convergence in the HDG domain.

Even though stable and accurate solutions are obtained in all cases, it is therefore recommended to use single-face approach as it is less sensitive to the value of parameter τ.

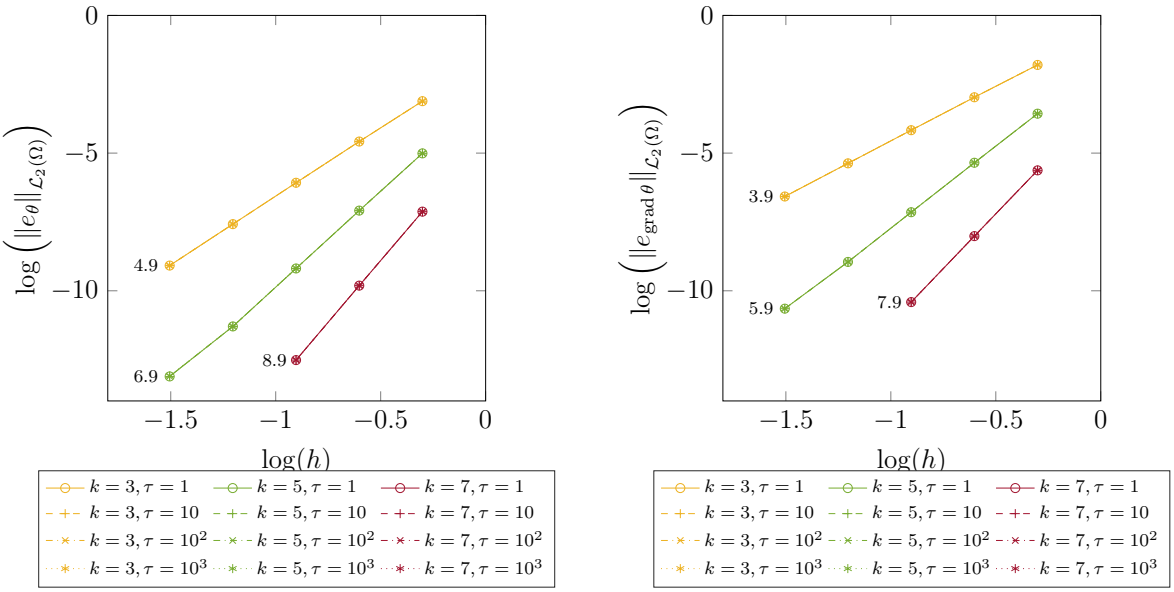

(a) θ. (b) grad θ.

Figure 6: Coupled CG(P_{k+1})-HDG(P_k): convergence of $\mathcal{L}_2$ norm of θ and grad θ in Ω showing the influence of parameter, τ, on coupled solution for single-face approach.

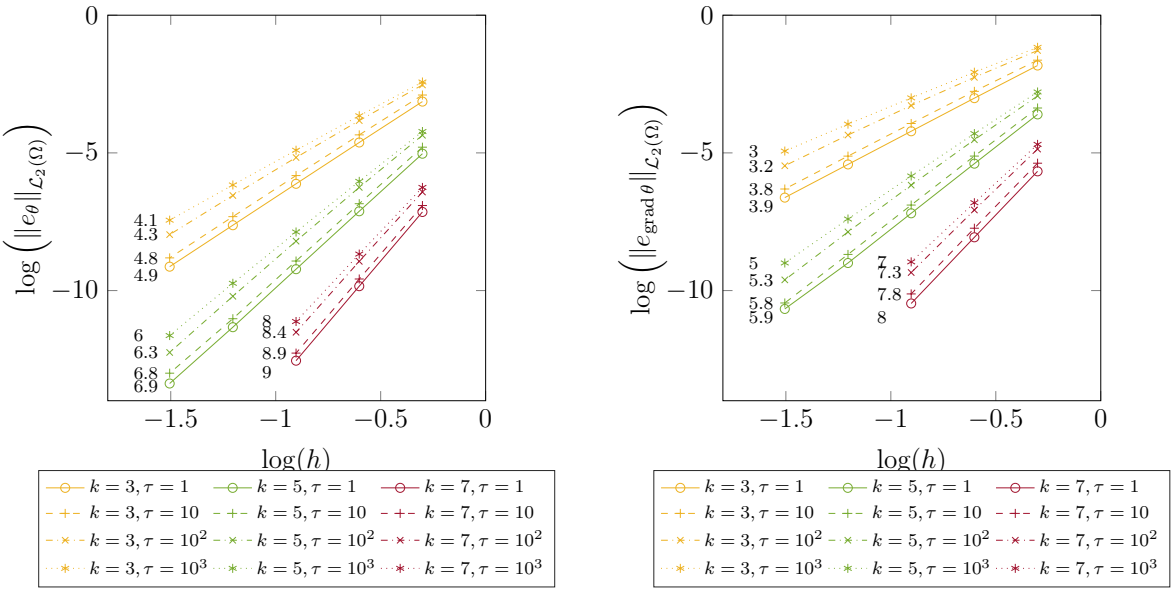

(a) θ. (b) grad θ.

Figure 7: Coupled CG(P_{k+1})-HDG(P_k): convergence $\mathcal{L}_2$ norm of θ and grad θ in Ω demonstrating the influence of parameter, τ, on coupled formulation for all-face approach.

4 CONCLUSIONS

Optimal HDG and CG convergence rates are kept with the proposed CG-HDG coupled formulation for the heat equation when the degree of approximation for CG is one degree higher than HDG degree. As expected, with the proposed CG-HDG coupled formulation, single-face approach is more robust with the variation of parameter τ than its all-face counterpart.

REFERENCES

[1] Cockburn, B., Dong, B., Guzmán, J.: A Superconvergent LDG-Hybridizable Galerkin Method for Second-Order Elliptic Problems. Mathematics of Computation **77**(264), 1887–1916 (2008)

[2] Cockburn, B., Dong, B., Guzman, J., Restelli, M., Sacco, R.: A hybridizable discontinuous Galerkin method for steady-state convection-diffusion-reaction problems. SIAM Journal on Scientific Computing **31**(5), 3827–3846 (2009)

[3] Cockburn, B., Gopalakrishnan, J., Lazarov, R.: Unified hybridization of discontinuous Galerkin, mixed, and continuous Galerkin methods for second order elliptic problems. SIAM Journal on Numerical Analysis **47**(2), 1319–1365 (2009)

[4] Cockburn, B., Guzmán, J., Wang, H.: Superconvergent discontinuous Galerkin methods for second-order elliptic problems. Mathematics of Computation **78**(265), 1–24 (2009)

[5] Giorgiani, G., Modesto, D., Fernández-Méndez, S., Huerta, A.: High-order continuous and discontinuous Galerkin methods for wave problems. International Journal for Numerical Methods in Fluids **73**(10), 883–903 (2013)

[6] Nguyen, N.C., Peraire, J., Cockburn, B.: An implicit high-order hybridizable discontinuous Galerkin method for the incompressible Navier–Stokes equations. Journal of Computational Physics **230**(4), 1147 – 1170 (2011)

[7] Paipuri, M.: Comparison and coupling of continuous and hybridizable discontinuous Galerkin methods: Applications to multi-physics problems. Ph.D. thesis, Instituto Superior Técnico, Universidade de Lisboa (2017)

[8] Paipuri, M., Fernández-Méndez, S., Tiago, C.: Comparison of high-order continuous and hybridizable discontinuous Galerkin methods in incompressible fluid flow problems. Mathematics and Computers in Simulation (2017). (Submitted)

[9] Reed, W.H., Hill, T.R.: Triangular mesh methods for the neutron transport equation. Los Alamos Report LA-UR-73-479 (1973)